NJC

PAPER

View Article Online
View Journal | View Issue

Cite this: *New J. Chem.*, 2017, **41**, 13846

Substituent swap affects the crystal structure and properties of *N*-benzyl-4-amino-1,2,4-triazole related organic salts†

Jing-Wen Wang, Yao-Jia Li, Chen Chen, Yang-Hui Luo * and Bai-Wang Sun *

Received 11th September 2017,
Accepted 6th October 2017

DOI: 10.1039/c7nj03445h

rsc.li/njc

An investigation into the effect of switching methoxy and hydroxyl groups on molecular salts is presented in this study. The salts $HL_1^+ \cdot NO_3^-$ (**1**), $L_1 \cdot HL_1^+ \cdot ClO_4^-$ (**2**), $L_1 \cdot HL_1^+ \cdot H_2PO_4^- \cdot H_2O$ (**3**), $HL_2^+ \cdot NO_3^-$ (**4**), $HL_2^+ \cdot ClO_4^-$ (**5**) and $HL_2^+ \cdot H_2PO_4^-$ (**6**) were synthesized and structurally characterized. The study was carried out by analyzing the crystal structure, properties and intermolecular interactions within each of the salts using IR and fluorescence spectra, TGA, Hirshfeld surface analyses and π···π stacking motifs. Salt **1** has a layered structure, while **4** has a distorted 3-D structure. Salt **2** possesses an edge-to-face type plane interaction, while **5** is formed with a twisted structure. It is important to note that water molecules play a key role in the 1-D chain structure of salt **3**. The π···π stacking motif of salts **1–3** have a herringbone structure, while salts **3–6** exhibit a γ-structure. In addition, the competitive crystallization of the synthetic salts was investigated and found to be consistent with the measured solubility.

1 Introduction

Anion receptors bearing π electron-deficient species have attracted increasing interest during the past decade.[1] The anion–π interaction, as predicted by researchers, has been shown to exist by experimental investigations involving electron-deficient aromatic rings in both solution and the solid state.[2–4] For example, in the solid state, when hydrogen-bonding interaction in which anions interact with π electron-deficient arenes, such as a benzene-capped tripodal amide ligand with a pyridyl moiety,[3a] *o*-CF_3 substituted hexaamide,[3b] and N4-platform-based polyamine tripodal[3c] from the periphery of the aromatic rings, is predominant, typical anion–π interaction, in which an anion (halide) is encapsulated in the middle of host molecule, is observed.[5] Despite an increasing number of examples of anion–π interactions being reported in the literature, to the best of our knowledge the effect of switching the substituents of the cationic species on the directing ability of the anion–π interaction based on charge-neutral, electron-deficient arenes has rarely been studied.

Inspired by studies carried out by Custelcean *et al.*[6,7] and Das *et al.*,[8] triazole-related ligands were selected for investigating anion–π interactions within inorganic acids due to their excellent hydrogen-bond acceptor and donor properties.[9,10] Moreover, the positive charge on the triazole group strengthens the oxoanion-binding through charge-assisted hydrogen bonding. In addition, our previous study has demonstrated that the binding ability of *N*-benzyl-4-amino-1,2,4-triazole-related ligands with inorganic anions can be affected remarkably by the substituent groups at the 4-position of the *N*-benzyl moiety.[10] In other words, the anion–π interactions between triazole-related ligands and anions can be controlled by altering the substituents on the triazole-related ligand.

Hence, two *N*-benzyl-4-amino-1,2,4-triazole related ligands L_1 and L_2 were synthesized and reacted with various inorganic acids (HNO_3, $HClO_4$, H_3PO_4) to form a series of salts, which form the focus of this study. A key aim of this article is to study the effect of exchanging the groups (methoxy and hydroxy) bound to the *para*-position of the *N*-benzyl ring, with a particular focus on how this affects the binding of the inorganic anions with L_1 and L_2, and therefore the spectral properties and stability of the resultant salts. The properties of the series of salts will be analyzed using TGA and IR, Raman and Fluorescence Spectroscopy. We qualitatively assess how changes in substitution influence the intra-molecular interactions of salts **1–6** and the position and presence of π···π stacking motifs. In addition, the competitive crystallization of the two ligands in the presence of nitrate, perchlorate and dihydrogen phosphate ions was also explored.

2 Experimental

2.1 General materials and methods

Nitric acid (HNO_3) (purity 65–68%), phosphoric acid (H_3PO_4) (purity ≥ 85 wt% in water) and perchloric acid ($HClO_4$)

School of Chemistry and Chemical Engineering, Southeast University, Nanjing 211189, P. R. China. E-mail: peluoyh@sina.com, chmsunbw@seu.edu.cn; Fax: +86-25-52090614; Tel: +86-25-52090614

† Electronic supplementary information (ESI) available. CCDC 1526868–1526874. For ESI and crystallographic data in CIF or other electronic format see DOI: 10.1039/c7nj03445h

(purity 70–72%) were purchased from Alfa Aesar and used without further purification. Infrared spectra (IR) was recorded on a SHIMADZU IR Prestige-21 FTIR-8400S spectrometer as KBr pellets in the range 4000–400 cm^{-1}. Thermogravimetric analysis (TGA) was performed using a NETZSCH TG 2009 F3 system, at a heating rate of 10 K min^{-1} under an atmosphere of dry nitrogen flowing at 20 cm^3 min^{-1} over the range from 50 to 500 °C. Elemental analyses were performed on a Vario-EL III elemental analyzer for carbon, hydrogen and nitrogen. NMR spectra were recorded on a Varian FT-400 MHz instrument. Fluorescence spectra were obtained using a Horiba FluoroMax 4 spectrofluorometer. Raman spectra were recorded using a Raman microscope (Kaiser Optical Systems, Inc., Ann Arbor, MI, USA) with 780 nm laser excitation; each spectrum was obtained under one 2 min exposure of the CCD detector in the wavenumber range.

Synthesis of ligand $C_{10}H_{10}N_4O_2$ (L_1). The ligands L_1, L_2 were synthesized according to methods described previously[11–13] (Scheme S1, ESI†). 4-Amino-4*H*-1,2,4-triazole (10 mmol, 0.84 g) was dissolved in 80 mL ethanol in a round-bottomed flask, and 3-hydroxy-4-methoxybenzaldehyde (10 mmol, 1.52 g) was added to the solution whilst under continuous stirring. The resulting solution was refluxed at 80 °C for 3 h. The solvent was removed under reduced pressure and the residue recrystallized from an ethanol solution (15 ml) by heating to 60 °C to dissolve solids and then leaving to cool (under ambient conditions). The resulting white, microcrystalline solid (L_1) was dried under vacuum conditions (2.00 g, yield 85%). Elemental analysis for L_1: Anal. calcd (%): C, 55.04; N, 25.68; H, 4.62. Found: C, 55.06; N, 25.64; H, 4.63. ^{1}H-NMR (300 MHz, d_6-DMSO) δ (ppm): 9.97(s, 1H), 9.04(s, 1H), 8.97(s, 2H), 7.52(d, 1H), 7.34(d, 1H), 6.35(s, 1H), 3.83(s, 3H) (see S1, ESI†).

Synthesis of ligand $C_{10}H_{10}N_4O_2$ (L_2). Ligand L_2 was prepared following a similar process as described above for L_1, except that the 3-hydroxy-4-methoxybenzaldehyde is replaced with 3-methoxy-4-hydroxybenzaldehyde (10 mmol, 1.52 g) to get a white solid product L_2 (2.00 g yield 85%).

Ligand L_1 was dissolved in a small amount of methanol solvent. The resulting clear solution was evaporated at room temperature over four days and colorless, blocky crystals of L_1, suitable for X-ray diffraction, were obtained. However, only the L_2 powder was collected for further measurements.

Synthesis of salts 1–3. The preparation of **1–3** was carried out in solution by slow evaporation-crystallization using pure methanol as solvent. Salt **1** was obtained by dissolving a 3 : 5 stoichiometric ratio of L_1 (45.60 mg, 0.3 mmol) and HNO_3 (48.46 mg, 0.5 mmol) in 20 mL methanol solution by continuously stirring for 20 minutes at room temperature. The resulting homogeneous solution was kept undisturbed at ambient temperature over four days to obtain a colorless transparent block crystal. The crystals of salts **2** and **3** were obtained in a similar way to that described for crystal **1**, with an identical stoichiometric ratio, but using $HClO_4$ (salt **2**) and H_3PO_4 (salt **3**) instead of HNO_3. Salts **1**, **2** and **3** were produced in 73–76%, 80–85%, 60–63% yields, respectively.

Synthesis of salts 4–6. Salt **4** was prepared by dissolving L_2 (45.60 mg, 0.3 mmol) and HNO_3 (48.46 mg, 0.5 mmol) in 20 ml methanol. The reaction mixture was stirred for 20 minutes, before being left undisturbed at ambient temperature for four days, whereupon an orange stick crystal of **4** was obtained *via* the low evaporation–crystallization process. Salts **5**, **6** were obtained using the same stoichiometric ratio, but using $HClO_4$ (salt **5**) and H_3PO_4 (salt **6**) instead of HNO_3, respectively. The yields of each salt were similar to those of salts **1–3** (IR is shown in Fig. S6, ESI†).

2.2 Competitive crystallizations of perchlorate/nitrate and perchlorate/dihydrogen phosphate

ClO_4^-/NO_3^-: 0.1 mmol ligand (L_1 or L_2) was dissolved in 10 mL of methanol, and then this solution was added to 10 mL of an aqueous solution of 0.1 mmol $HClO_4$ and 0.1 mmol HNO_3. The resulting mixture was then stirred at room temperature for 24 h, during which a colorless crystalline solid was formed. The resulting crystalline solid was filtered, washed with water, and dried under vacuum to provide the product in a yield of 55–60%; PXRD and FT-IR analyses were performed to elucidate the composition of the crystalline solid.

$ClO_4^-/H_2PO_4^-$: competitive crystallizations of $ClO_4^-/H_2PO_4^-$ were performed by similar procedures as described above, except that H_3PO_4 was used instead of HNO_3. Again, PXRD measurements were performed to investigate the composition of the crystalline solid. Yield 58–62%.

2.3 X-ray crystallography

Crystallographic diffraction of L_1 and salts **1–6** was performed at 293 K with graphite-monochromated Mo Ka radiation (λ = 0.071073 nm) equipped with Rigaku SCXmini diffractometer, using the ω-scan technique.[14] The absorption correction was carried out using the Bruker SADABS program with a multi-scan method. The structures were solved by full-matrix least-squares methods on all F^2 data, and the SHELXS-2014 and SHELXL-2014 programs were used for the structure solution and structure refinement, respectively.[15] All non-hydrogen atoms were refined anisotropically and hydrogen atoms (except the hydrogen atoms from the water molecule) were inserted at their calculated positions and fixed at their positions.[16] Mercury program[17] was used to produce the molecular graphics. Further details of the crystallographic data and structural refinement results of the L_1 and salts **1–6** are given in Table S1 (ESI†), and selected H-bond lengths and angles of ligand L_1 and salts **1–6** are listed in Table S2 (ESI†).

2.4 The Hirshfeld surface

The Hirshfeld surface serves as a powerful tool for elucidating molecular crystal structures,[18,19] and is determined using the CrystalExplorer26 program in this study. When the CIF files were read into the CrystalExplorer program for analysis, all bond lengths to hydrogen were automatically modified to typical standard neutron values (C–H = 1.083 Å and N–H = 1.009 Å). The Hirshfeld surfaces were generated using standard (high) surface resolution, and the 3-D de surfaces were mapped using a fixed color scale of 0.76 Å (red) to 2.4 Å (blue). The 2-D fingerprint plots were displayed using the standard 0.6–2.6 Å

view with the de and di distance scales displayed on the graph axes.

3 Results and discussion

3.1 Description of crystal structures

$C_{10}H_{10}N_4O_2$ (L_1). Ligand L_1 crystallizes in the monoclinic space group *P*21/*c*, revealing a 1-D O2–H2A···N2 hydrogen bond-interaction structure. As shown in Fig. 1a, the asymmetric unit consists of only one L_1 molecular. The O2–H2A···N2 bond length is 2.72 Å, which is comparable to what has been previously reported for O–H···N hydrogen bonding in compounds with similar structures (Fig. S2, ESI†). From the view of Fig. 1b, the L_1 molecules interact with each other *via* hydrogen bonds, forming a cross-connected structure; the cross-connected structures experience additional stacking due to π···π intermolecular interactions, ultimately creating an interlaced 3-D layer structure. The plane separation between the stacked L_1 molecules in the adjacent units is 4.165 Å and 3.498 Å in the horizontal direction and tilt direction, respectively.

Salts $HL_1^+ \cdot NO_3^-$ (**1**) and $HL_2^+ \cdot NO_3^-$ (**4**). Single-crystal X-ray diffraction analysis reveals that salt **1** crystallizes in the monoclinic space group *P*21/*c*, showing a 2-D network structure. As shown in Fig. 2a, the asymmetric unit of salt **1** contains a single molecule of protonated HL_1^+ per nitrate ion. The ASU of salt **4** is similar to that of salt **1**, consisting of a molecule of protonated HL_2^+ per nitrate ion. Salt **4** crystallizes in the monoclinic space group *Pn*. The structure of **4** is different from that of **1** owing to the position switch of the methoxy and hydroxyl groups. Salt **1** is mainly stabilized by intramolecular O5–H5A···O2 and N5–H5···O3 hydrogen bonds and is stacked in a parallel fashion, forming a layered 3-D structure held together by π···π intermolecular interactions with a plane separation of 3.497 Å (Fig. 2c). The absence of interaction between the methoxy group and the N atom of another ligand molecule leads to a completely different crystal structure of salt **1** compared to that of salt **4**. Salt **4** is mainly held together by N1–H1B···O1 and N1–H1B···O2 hydrogen bonding interactions: the oxygen atoms of the methoxy and hydroxyl groups are involved in the formation of the structure by hydrogen bonding. The 3-D packing of salt **4** shows that the layers are not parallel to each other (Fig. 2d).

$L_1 \cdot HL_1^+ \cdot ClO4^-$ (**2**) and $HL_2^+ \cdot ClO_4^-$ (**5**). As shown in Fig. 3a, salt **2** crystallizes in the triclinic space group $P\bar{1}$, the ASU contains one L_1 molecule (neutral), one protonated HL_1^+ and one perchlorate ion. Compared with salt **2**, the structure of **5** has a 1 : 1 (L_2: perchloric acid) molecular salt in the monoclinic *Pn* space group with $Z = 2$ and the ASU consists of a protonated molecule of HL_2^+ and a perchlorate ion (Fig. 3b).

For salt **2**, each protonated molecule of HL_1^+ is connected by O1–H1A···N1, N6–H6···N2 and O3–H3B···O5 interactions to form an edge-to-face type plane structure (Fig. S4a, ESI†). The 2-D plane structures are then stacked in a bridged fashion of the perchlorate ion by C–H···π weak intermolecular hydrogen bonds into the layered structures (Fig. 3c). In this regard, salt **5** shows a visible difference from **2**. Single-crystal X-ray diffraction analysis showed that the protonated HL_2^+ molecules in salt **5** have twisted structures (they are not 'flat'), with the 3-D structure held together *via* O1···O6 lone electron pair, and N1–H1···O2 and O1–H1A···N1 hydrogen bonding interactions (Fig. 3d). Compared with **2**, both methoxy and hydroxyl groups in salt **5** participate in the formation of the packing structure *via* strong O–H···N interactions.

$L_1 \cdot HL_1^+ \cdot H_2PO_4^- \cdot H_2O$ (**3**) and $HL_2^+ \cdot H_2PO_4^-$ (**6**). Salt **3** features a 3-D anionic network based on dihydrogen phosphate ions. Single-crystal X-ray diffraction analysis reveals that salt **3** crystallizes in the orthorhombic space group *Pca*21. As shown in Fig. 4a, each asymmetric unit of salt **3** contains one dihydrogen phosphate ions, one neutral L_1 molecule, one protonated HL_1^+ and one lattice water. Compared to that of salt **3**, there is no water in the ASU of salt **6**, and it only consists of one protonated HL_2^+ and one dihydrogen phosphate ion in the monoclinic space group *Pn*.

The structure of salt **3** can be described as follows: the molecules of protonated HL_1^+ are connected through N8–H8A···O2 (distance of 2.61 Å) and O5–H5···O3 (distance of 2.64 Å) hydrogen bonds, with the water molecules playing an important bridging role by connecting the two dihydrogen phosphate ions in a 1-D chain structure through numerous O1–H1A···O2W and O2W–H···O2 hydrogen bonds (Fig. S5a, ESI†).

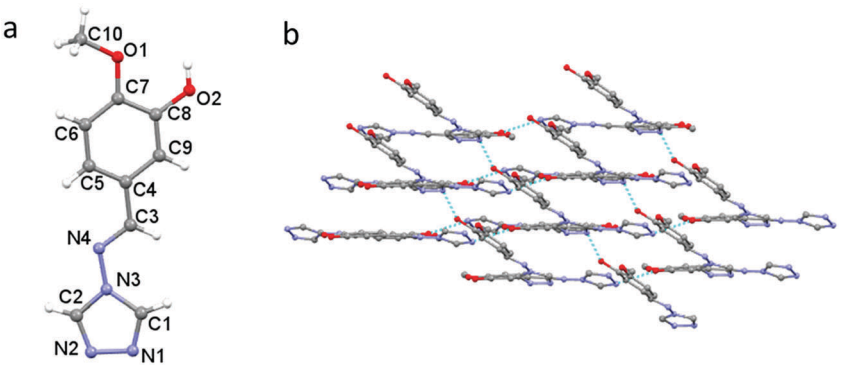

Fig. 1 (a) The asymmetric unit of ligand L_1 with the atomic labeling scheme. (b) Hydrogen bonding patterns of L_1; the hydrogen atoms are omitted for clarity.

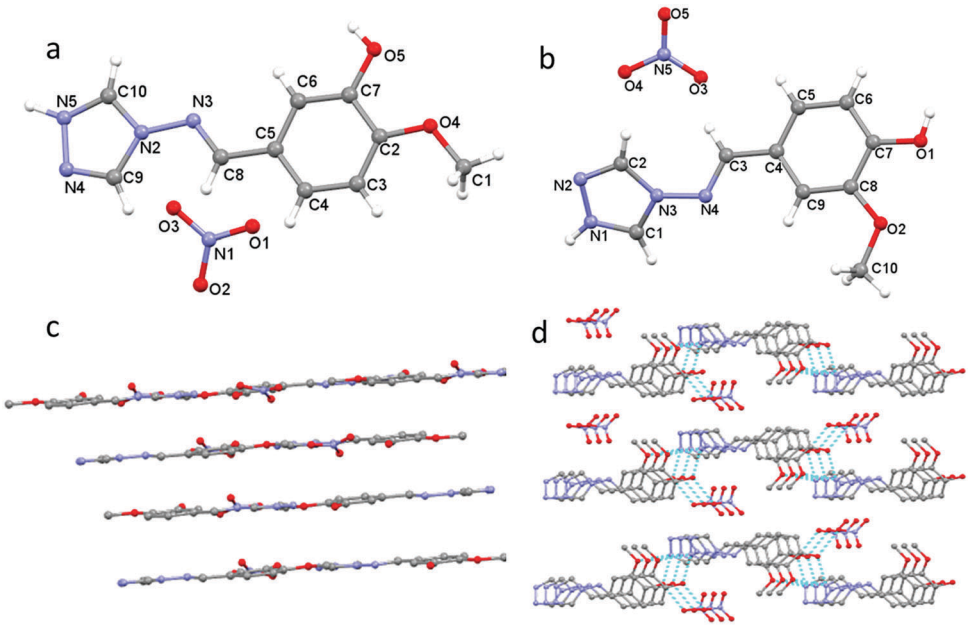

Fig. 2 X-ray crystal structure of the salts **1** and **4**. ORTEP representation showing (a) the structure of the cation and (b) the structure of the anion. (c) The crystal packing of salt **1** viewed along the *b*-axis. (d) The crystal packing of salt **4**, as viewed along the a-axis, and with the intermolecular hydrogen bond interactions highlighted (pale blue dotted marking). The hydrogen atoms have been omitted for clarity.

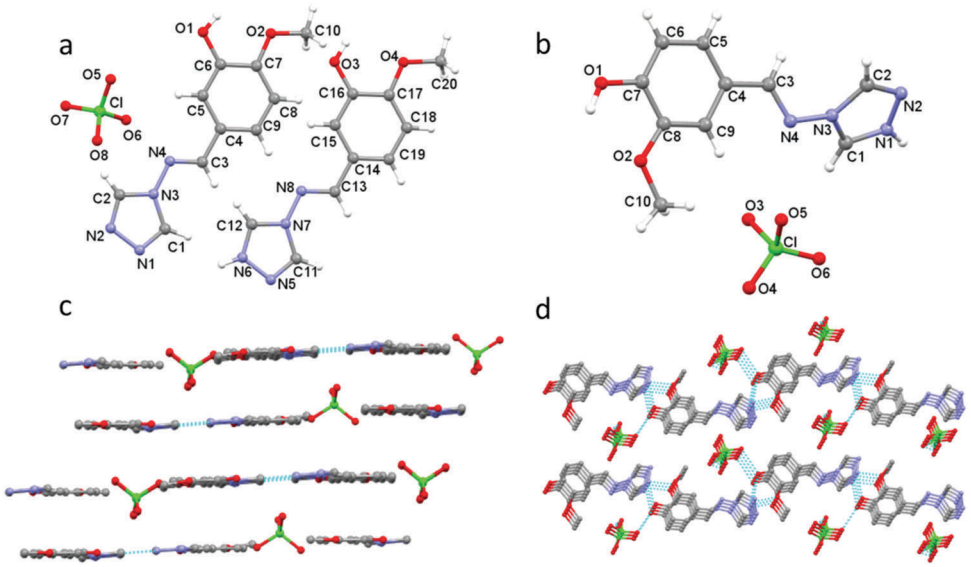

Fig. 3 (a) The asymmetric unit of salts **2** and **5** with the atomic labeling scheme (a and b). 3-D pack structure of salts **2** (c). Crystal packing of salt **5**, viewed down the crystallographic *a*-axis (d). The hydrogen atoms are omitted for clarity.

Salt **3** forms an edge-to-edge type interaction, with the dihydrogen phosphate ions located on the inner position of the opposite chain unit, while the protonated HL_1^+ molecules are on the two sides (Fig. 4c). The structure of salt **6**, is largely constructed of direct N3–H3A···O1 and N3–H3A···O6 hydrogen bonds, which originate in L_2. In addition, **6** forms edge-to-face type interactions, which are similar to those found in salts **4** and **5**. The dihydrogen phosphate ions are located on the inner position of the reversed chain unit, while the protonated HL_2^+ molecules are on the two sides. Furthermore, the 3-D structures of salts **3** and **6** show a significant difference, as can be observed in Fig. 4c and d. This difference can be ascribed to the position swap of methoxy and hydroxyl groups between ligands L_1 and L_2. The hydrogen bond interactions of ligand L_1 and salts **1–6** are shown in Fig. S2–S5 (ESI†).

3.2 The influence of the positional switching of the methoxy and hydroxyl groups on the structure and spectral properties of ligands L_1, L_2 and salts 1–6

As is shown in Fig. 5, a comparison of the structures of salts **1–6** shows that the hydrogen bond connection mode of the

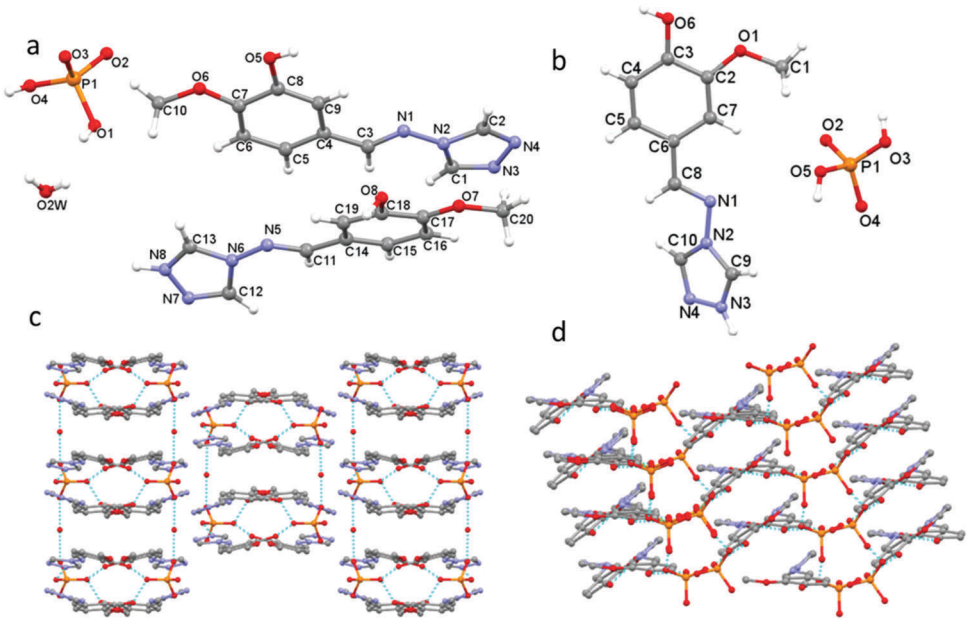

Fig. 4 The asymmetric unit of (a) salt **3** and (b) salt **6**, showing the atomic labeling scheme. The crystal structures of (c) salt **3** and (d) salt **6**, viewed down the crystallographic *c*-axis. The hydrogen atoms are omitted for clarity (a–d).

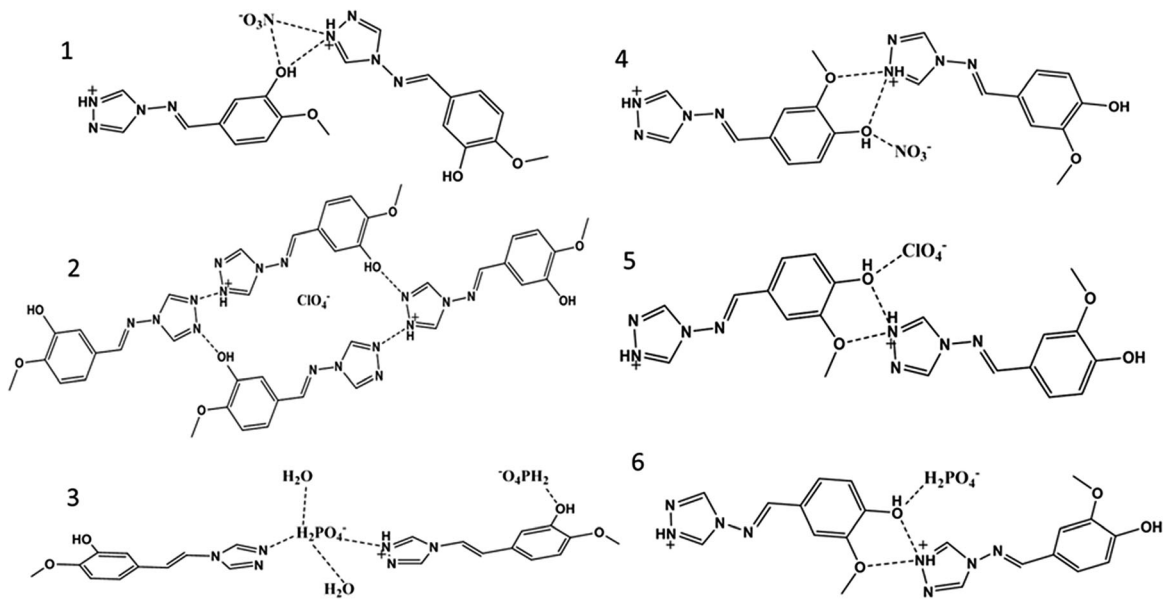

Fig. 5 Hydrogen bonding patterns of the ligand L_1/L_2 stacks with inorganic anions to form salts **1–6**.

inorganic anions with ligands L_1 and L_2 has a profound effect on the overall structure of each salt. The same ligand can be connected with different anions to form different structures, and the same anion can also be connected with different ligands to form different salt structures. In salt **1**, each nitrate ion interacts with three neighboring protonated HL_1^+ species, forming a 2-D network plane (Fig. 2c), with each hydroxyl group of L_1 forming two hydrogen bonds (N5–H5···O3 and O5–H5A···O2), while the hydroxyl group in L_2 forms a O1–H1A···O4 hydrogen bond within salt **4** (Fig. S3, ESI†). The nitrate ion in salt **4** interacts with five protonated HL_2^+ molecules, two above and two below the main plane, forming an overall twisted 2-D structure. In salt **2**, there are two independent L_1 molecules connected through O1–H1A···N1 and N6–H6···N2 hydrogen bonds; beyond that, the perchlorate anion interacts with L_1 by weak hydrogen bonds. However, perchlorate anions interact strongly with the hydroxyl group in salt **5** *via* hydrogen bonding, and O3 and O5 (between the perchlorate groups) can also be connected by lone electron pairs. For salts **3** and **6**, the main difference is that **3** contains

lattice water, and dihydrogen phosphate ions are linked by water molecules whilst for salt **6**, the dihydrogen phosphate ions are connected directly without water. Thus, the position swap of methoxy and hydroxyl groups on L_1 and L_2 results in distinct crystal packing structures (Fig. 5).

The solution-state emission spectra of compounds L_1, L_2 and salts **1–6** at ambient temperature are shown in Fig. 6. The main emission peaks of the ligands L_1 and L_2 are at 415 nm (λ_{ex} = 321 nm) and 400 nm (λ_{ex} = 320 nm), respectively, which may be due to π*–π or π*–n intra-molecular transitions. The same emissions occur at 420 nm for **1**, 420 nm for **2**, 414 nm for **3**, 427 nm for **4**, 433 nm for **5** and 403 nm for **6** (λ_{ex} = 322 nm). The emissions of these salts may be assigned to the conjugate effects of intra-molecular transitions and differences in the conjugate environments. As is shown in Fig. 6, the fluorescence wavelength of L_1 is longer than that of L_2, which may be ascribed to the molecular structure of L_1 on the same plane. Compared to the free L_1 and L_2 ligands, the peaks are red-shifted by 5 nm, 5 nm, 27 nm and 33 nm for salts **1**, **2**, **4**, **5**, respectively. It can be seen that when NO_3^- and ClO_4^- are associated with L_2, the emission has a larger fluorescence shift, because the methoxy and hydroxyl groups in the L_2 are all linked by hydrogen bonding with the oxo-anion, thereby increasing the conjugation capacity (Fig. 5). The emission peaks for salts **3** and **6** are essentially the same as the corresponding ligand, which implies that $H_2PO_4^-$ has little effect on the fluorescence emission of the ligands.

3.3 Competitive crystallization

According to the above mentioned crystallization experiments, it is apparent that both the ligands L_1 and L_2 can generate relatively insoluble salts with various oxoanions, providing a range of yields. This caused us to investigate the potential for selective oxoanion separation using the two *N*-benzyl-4-amino-1,2,4-triazole related ligands (L_1 and L_2). Table S3 (ESI†) lists the measured aqueous solubilities of the dihydrogen phosphate, nitrate and perchlorate salts at 25 °C. The salts decrease in their solubility in the order dihydrogen phosphate salts > nitrate salts > perchlorate salts. Thus, perchlorate salts have the lowest aqueous solubility, indicating the possibility of aqueous perchlorate separation *via* selective crystallization of the salts $L_1{\cdot}HL_1^+{\cdot}ClO_4^-$ and $HL_2^+{\cdot}ClO_4^-$.

To verify the abovementioned proposition, a series of competitive crystallization experiments were performed involving the crystallization of ligands L_1 and L_2 in aqueous solution in the presence of various anion mixtures (Table S4, ESI†). The composition of the resulting crystalline products was confirmed by PXRD and FT-IR measurements. For ligand L_1, salt $L_1{\cdot}HL_1^+{\cdot}ClO4^-$ (**2**) was exclusively crystallized from the perchlorate/nitrate and perchlorate/dihydrogen phosphate mixtures in 76% and 78% yield, respectively (entries 1–2), while for ligand L_2, crystalline mixtures of $HL_2^+{\cdot}NO_3^-$ (**4**) and $HL_2^+{\cdot}ClO_4^-$ (**5**) as well as $HL_2^+{\cdot}H_2PO_4^-$ (**6**) and $HL_2^+{\cdot}ClO_4^-$ were obtained from the 'competition experiment' using perchlorate/nitrate and perchlorate/dihydrogen phosphate, respectively (entries 3–4). These results may be attributed to the similar crystal structures and aqueous solubilities of the salts **1**, **2** and **3**. Thus, the anion selectivity from these paired competitive crystallizations are generally consistent with the measured solubilities.

3.4 The Hirshfeld surface

The effects of switching methoxy and hydroxyl groups on L_1, L_2 can also be visualised by the Hirshfeld surface, which is a useful tool for describing the surface characteristics of

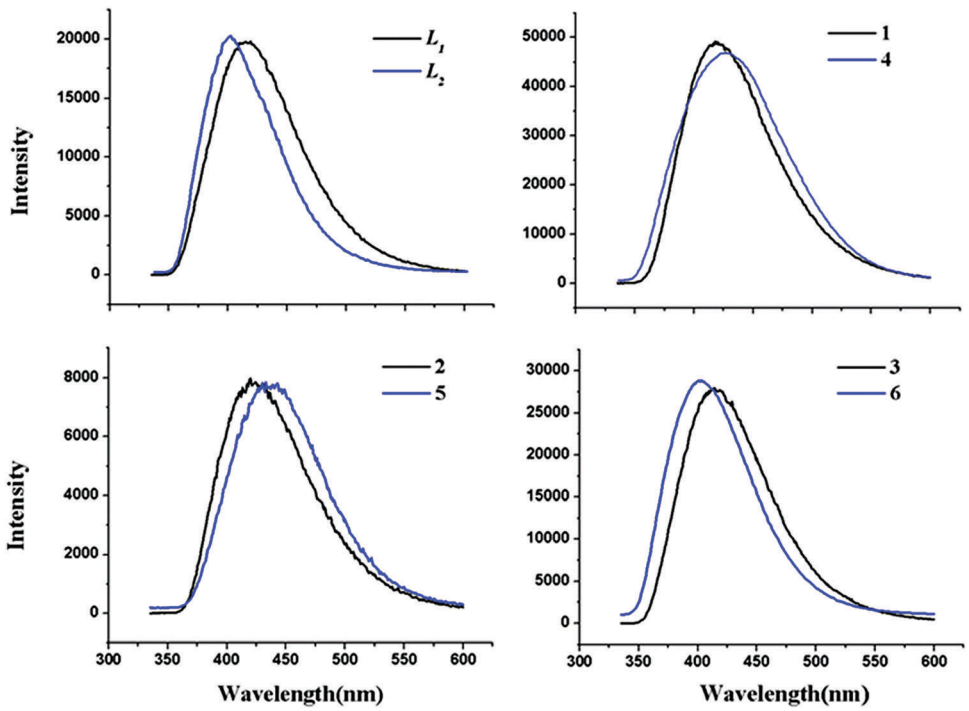

Fig. 6 Fluorescence emission spectra of ligands L_1, L_2 and salts **1–6** (λ_{ex} = 322 nm, $c = 2.5 \times 10^{-5}$).

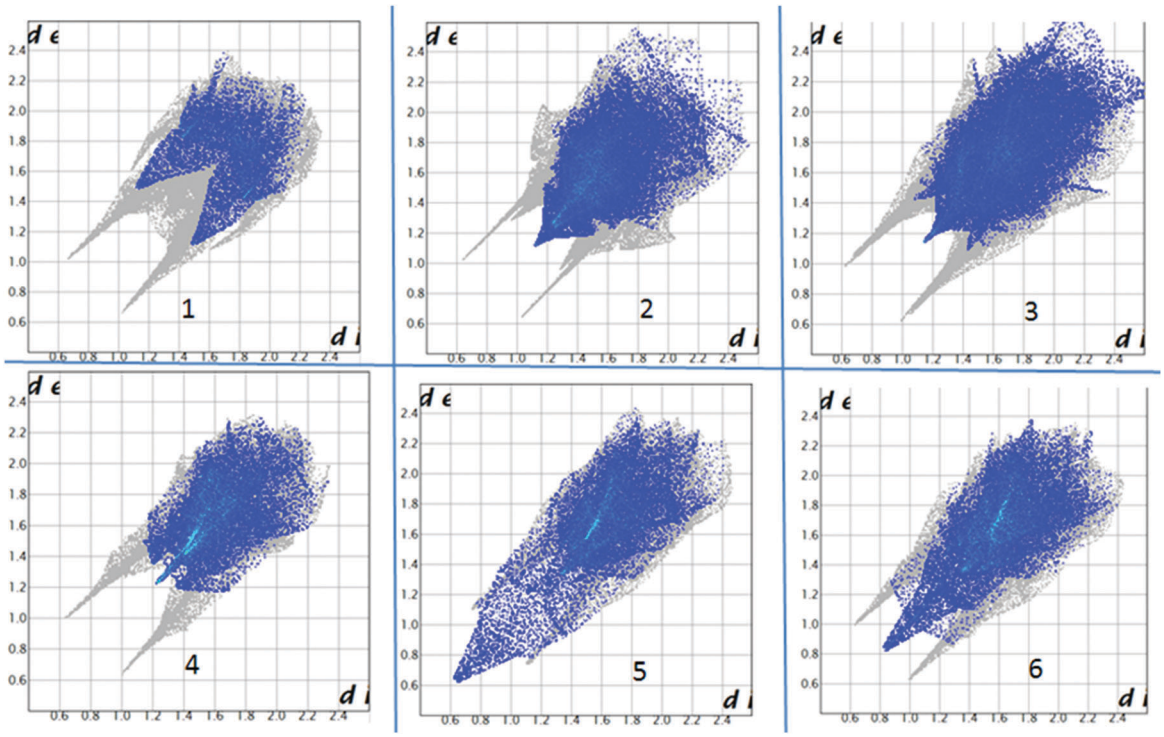

Fig. 7 Fingerprint plots for salts **1–6** resolved into H···H interaction, the full fingerprint appears beneath each decomposed plot as a grey shadow.

molecules. All the intermolecular interactions within salts **1–6** are summarized in Fig. 8, which enables the influence of substituent position and different inorganic anions on the intermolecular interactions to be more fully appreciated. The H···O interaction, which forms the greatest contribution to the total Hirshfeld surface, comprises 45.6%, 33.1%, 39.0%, 37.6%, 35.3% and 35.6% of the total Hirshfeld surfaces for salts **1–6**, respectively. Compared to other salts, salt 2 has a significantly lower value; this can be explained by the fact that N···H interactions in salt **2** play an obvious role in the construction of the structure (Fig. 5). Furthermore, the O···O interaction, which comprises 7.8% of the total Hirshfeld surface, also has a unique role in the connection of perchlorate ions in salt **2**. Interestingly, the C···O interaction contributes 1.9%, 2.9%, 4.1%, 5.4% and 5.6% of the total Hirshfeld surfaces for salts **1**, **2**, **4**, **5**, **6**, respectively, with the exception of salt **3**, due to the bridging effects of water molecules. The H···H contacts comprise 17.9%, 23.2%, 26.6%, 23.2%, 23.3%, and 29.3% of the total Hirshfeld surfaces for salts **1–6**, respectively. It can be seen that the values depend strongly on the substituent position of the methoxy and hydroxyl groups (Fig. 7).

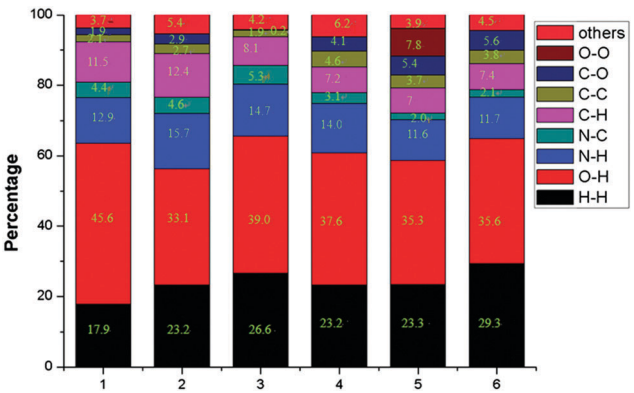

Fig. 8 The percentage contributions from the individual intermolecular interactions to the Hirshfeld surfaces of salts **1–6**.

3.5 The π···π stacking motifs

Aromatic compounds usually crystallize in one of four possible structural motifs: herringbone, sandwich-herringbone, γ-, or β-structures (Fig. 9).[20–22] The determination of structural motifs is based on the calculated ratios between C–H···π and π···π (C···C) interactions. According to the literature,[22] herringbone structures have a ratio greater than 4.5, sandwich-herringbone structures have a ratio between 3.2 and 4.0, γ-structures have ratios in the range 1.2–2.7, and β-structures have a ratio between 0.46 and 1.0. The ratios of salts **1–6** are found to be 5.47, 4.59, 4.26, 1.56, 1.89 and 1.94, respectively; *i.e.*, the π···π stacking motif of salts **1–3** has a herringbone structure whilst salts **4–6** have a γ-structure. According to Desiraju and Gavezzotti,[21] each motif represents a particular π-interaction geometry: the herringbone-motifs are rich in C–H···π interactions and often form edge-to-face interactions, while the γ-motifs are rich in π···π (C···C) interactions and the molecules in them often form infinite face-to-face or offset stacks along one axis and edge-to-face stacks along another axis. This implies that different types of inorganic anions have little effect on π···π stacking motifs, whereas the substituted positions make a big difference to the π···π stacking motifs of organic salts.

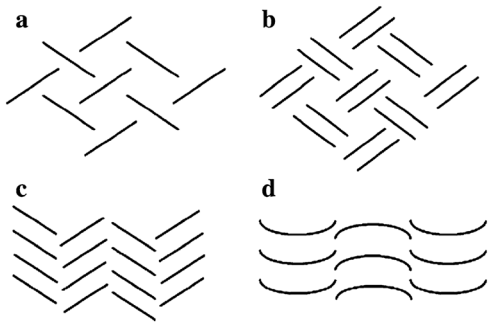

Fig. 9 Diagrammatic representation of the (a) herringbone, (b) sandwich-herringbone, (c) γ (g), and (d) β (b) packing motifs.

3.6 Thermogravimetric analysis (TGA) of ligands L_1, L_2 and salts 1–6

The thermogravimetric behaviors of the ligands and salts are shown in Fig. S8 (ESI†). Compounds L_1 and L_2 start to decompose at 232 °C and 235 °C, respectively. Salts **1** and **4** undergo two sets of mass loss (in steps) at temperatures of 135 °C and 157 °C, respectively. The first weight loss step is mainly due to the decomposition of nitrate and further weight loss can be attributed to the decomposition of HL_1^+/HL_2^+ fragments and the collapse of the lattice structure. The decomposition temperature of nitrate in salts **1** and **4** is considerably lower than that of the corresponding ligands L_1 and L_2. The other four salts undergo a one-step mass loss at temperatures of 232, 223, 242 and 247 °C for salts **2**, **3**, **5**, and **6**, respectively, and these decomposition temperatures are similar to those of the corresponding ligands. Thus, the different substituted positions have little effect on the decomposition temperature, while the different types of inorganic anions affect the thermal decomposition temperature of the salts substantially.

4 Conclusions

In summary, a series of organic salts $HL_1^+\cdot NO_3^-$ (**1**), $L_1\cdot HL_1^+\cdot ClO4^-$ (**2**), $L_1\cdot HL_1^+\cdot H_2PO_4^-\cdot H_2O$ (**3**), $HL_2^+\cdot NO_3^-$ (**4**), $HL_2^+\cdot ClO_4^-$ (**5**) and $HL_2^+\cdot H_2PO_4^-$ (**6**) based on simple *N*-benzyl-4-amino-1,2,4-triazole related ligands have been designed, synthesized and studied. Compound **1** exhibits a layered 3-D structure through π···π interaction, while salt **4** shows a twisted packing structure. For salts **2** and **5**, hydrogen-bonding interactions play a large role in the overall crystal structure. Compared with salt **3**, in which water molecules link to dihydrogen phosphate ions resulting in an infinite 1-D chain, salt **6** molecules are connected directly *via* dihydrogen phosphate ions. The luminescence properties reveal that the presence of dihydrogen phosphate ions maintains the emission wavelength of the ligand (*i.e.*, in salts **3** and **6**), while the presence of nitrate and perchlorate ions results in an increase in the emission wavelength in the corresponding salts (**1**, **2** and **4**, **5**, respectively). The C···O interactions are not present in salt **3**, and the O···O interactions are present in salt **5**. The π···π stacking motifs change from herringbone (salts **1–3**) to γ-motifs (salts **4–6**), and the anion selectivity from the abovementioned pairwise competitive crystallizations are generally consistent with the measured solubilities.

Conflicts of interest

There are no conflicts to declare.

Acknowledgements

This research was supported by the Natural Science Foundation of China (Grant no. 21371031 and 21628101), the International S&T Cooperation Program of China (No. 2015DFG42240) and the Priority Academic Program Development (PAPD) of Jiangsu Higher Education Institutions.

References

1 (*a*) L. M. Salonen, M. Ellermann and F. Diederich, *Angew. Chem., Int. Ed.*, 2011, **50**, 4808; (*b*) P. Gamez, T. J. Mooibroek, S. J. Teat and J. Reedijk, *Acc. Chem. Res.*, 2007, **40**, 435; (*c*) B. J. Kristin, A. Bianchi and E. García-España, *Anion coordination chemistry*, Wiley-VCH, 2012, pp. 141–225.
2 D. Kim, P. Tarakeshwar and K. S. Kim, *J. Phys. Chem. A*, 2004, **108**, 1250.
3 (*a*) S. Chakraborty, R. Dutta, M. Arunachalam and P. Ghosh, *Dalton Trans.*, 2014, **43**, 2061; (*b*) S. Chakraborty, R. Dutta, B. M. Wong and P. Ghosh, *RSC Adv.*, 2014, **4**, 62689; (*c*) M. N. Hoque and G. Das, *CrystEngComm*, 2014, **16**, 4447.
4 (*a*) Y. H. Luo, J. W. Wang, Y. J. Li, C. Chen, P. J. An, S. L. Wang, C. Q. You and B. W. Sun, *CrystEngComm*, 2017, **19**, 3362; (*b*) S. Dalapati, M. A. Alam, S. Janaa and N. Guchhait, *CrystEngComm*, 2012, **14**, 6029; (*c*) M. N. Hoque, A. Basu and G. Das, *Cryst. Growth Des.*, 2014, **14**, 6; (*d*) T. Hu, X. Zhao, X. Hu, Y. Xu, D. Sun and D. Sun, *RSC Adv.*, 2011, **1**, 1682.
5 D. X. Wang, S. X. Fa, Y. Liu, B. Y. Hou and M. X. Wang, *Chem. Commun.*, 2012, **48**, 11458.
6 R. Custelcean, N. J. Williams and C. A. Seipp, *Angew. Chem., Int. Ed.*, 2015, **54**, 10525.
7 R. Custelcean, N. J. Williams, C. A. Seipp, A. S. Ivanov and V. S. Bryantsev, *Chem. – Eur. J.*, 2016, **22**, 1997.
8 M. N. Hoque and G. Das, *CrystEngComm*, 2017, **19**, 1343.
9 (*a*) Y. Garcia, V. Niel, M. C. Munoz and J. A. Real, *Top. Curr. Chem.*, 2004, **233**, 229; (*b*) T. Sergeieva, M. Bilichenko, S. Holodnyak, Y. V. Monaykina, S. I. Okovytyy, S. I. Kovalenko, E. Voronkov and J. Leszczynski, *J. Phys. Chem. A*, 2016, **120**, 10116.
10 (*a*) Y.-H. Luo, D.-E. Wu, G.-J. Wen, L.-S. Gu, L. Chen, J.-W. Wang and B.-W. Sun, *ChemistrySelect*, 2017, **2**, 61; (*b*) J. W. Wang, C. Chen, Y. J. Li, Y. H. Luo and B. W. Sun, *New J. Chem.*, 2017, **41**, 9444.
11 (*a*) B. Belghoul, I. Welterlich, A. Maier, A. Toutianoush, A. R. Rabindranath and B. Tieke, *Langmuir*, 2007, **23**, 5062;

(*b*) P. S. Hariharan and S. P. Anthony, *Anal. Chim. Acta*, 2014, **848**, 74; (*c*) C. C. Núñez, S. López, O. N. Faza, F. L. Javier, M. Diniz, R. Bastida, J. L. Capelo and C. Lodeiro, *J. Biol. Inorg. Chem.*, 2013, **18**, 679.

12 H. Yuan, Q. Q. Li, H. Li, Q. N. Guo, Y. G. Lu and Z. Y. Li, *Dalton Trans.*, 2010, **39**, 11344.

13 H. D. Bian, W. Gu, J. Y. Xu, F. Bian, S. P. Yan, D. Z. Liao, Z. H. Jiang and P. Cheng, *Inorg. Chem.*, 2003, **42**, 4265.

14 Rigaku, CrystalClear, Version 14.0, Rigaku Corporation, Tokyo, Japan, 2005.

15 G. M. Sheldrick, *SHELXS97, Programs for Crystal Structure Analysis*, University of Göttingen, Germany, 1997.

16 (*a*) Y.-H. Luo, C. Chen, Y.-J. Li, J.-W. Wang and B.-W. Sun, *Dyes Pigm.*, 2017, **143**, 239; (*b*) J.-W. Wang, Y.-W. Zhang, M.-X. Wang, Y.-H. Luo and B.-W. Sun, *Polyhedron*, 2017, **124**, 243.

17 Mercury 2.3 Supplied with Cambridge Structural Database, CCDC, Cambridge, UK, 2003–2004.

18 (*a*) J. J. McKinnon, A. S. Mitchell and M. A. Spackman, *Chem. – Eur. J.*, 1998, **4**, 2136; (*b*) M. A. Spackman and J. J. McKinnon, *CrystEngComm*, 2002, **4**, 378.

19 J. J. McKinnon, M. A. Spackman and A. S. Mitchell, *Acta Crystallogr., Sect. B: Struct. Sci.*, 2004, **60**, 627.

20 G. R. Desiraju and A. Gavezzotti, *Acta Crystallogr., Sect. B: Struct. Sci.*, 1989, **45**, 473.

21 G. R. Desiraju and A. Gavezzotti, *J. Chem. Soc., Chem. Commun.*, 1989, 621–623.

22 L. Loots and L. J. Barbour, *CrystEngComm*, 2012, **14**, 300.

